

Article

Application of an Image Tracking Algorithm in Fire Ant Motion Experiment

Lichuan Gui ^{*} and John M. Seiner

National Center for Physical Acoustics (NCPA), University of Mississippi, 1 Coliseum Drive, University, MS 38677, United States

^{*} Author to whom correspondence should be addressed: lcgui@olemiss.edu

Received: 26 March 2009; in revised form: 23 April 2009 / Accepted: 24 April 2009 /

Published: 30 April 2009

Abstract: An image tracking algorithm, which was originally used with the particle image velocimetry (PIV) to determine velocities of buoyant solid particles in water, is modified and applied in the presented work to detect motion of fire ant on a planar surface. A group of fire ant workers are put to the bottom of a tub and excited with vibration of selected frequency and intensity. The moving fire ants are captured with an image system that successively acquires image frames of high digital resolution. The background noise in the imaging recordings is extracted by averaging hundreds of frames and removed from each frame. The individual fire ant images are identified with a recursive digital filter, and then they are tracked between frames according to the size, brightness, shape, and orientation angle of the ant image. The speed of an individual ant is determined with the displacement of its images and the time interval between frames. The trail of the individual fire ant is determined with the image tracking results, and a statistical analysis is conducted for all the fire ants in the group. The purpose of the experiment is to investigate the response of fire ants to the substrate vibration. Test results indicate that the fire ants move faster after being excited, but the number of active ones are not increased even after a strong excitation.

Keywords: image tracking, image identification, fire ant, PIV, PTV

1. Introduction

A vibration-based technique is under development at the University of Mississippi's National Center for Physical Acoustics (NCPA) for inducing motion of black imported fire ants (BIFAs) in a tub. The tub is normally situated inside of large "attack boxes" used by research entomologists at the Biological Control of Pests Research Unit (BCPRU) in Stoneville, Mississippi, to provide an arena whereby worker ants are exposed to attacks by parasitoid phorid flies (*Pseudacteon curvatus* Borgmeier) in a dedicated effort to increase artificial mass production of phorid fly pupae inside the bodies of fire ant workers [1, 2]. In order to quantify the distribution and motion of the fire ants in the tub, a digital imaging system is used to record successive image frames of fire ants on the tub bottom surface. The digital ant image recordings are processed in a similar way to those for processing particle image velocimetry (PIV) recordings of low-image-density (LID) mode.

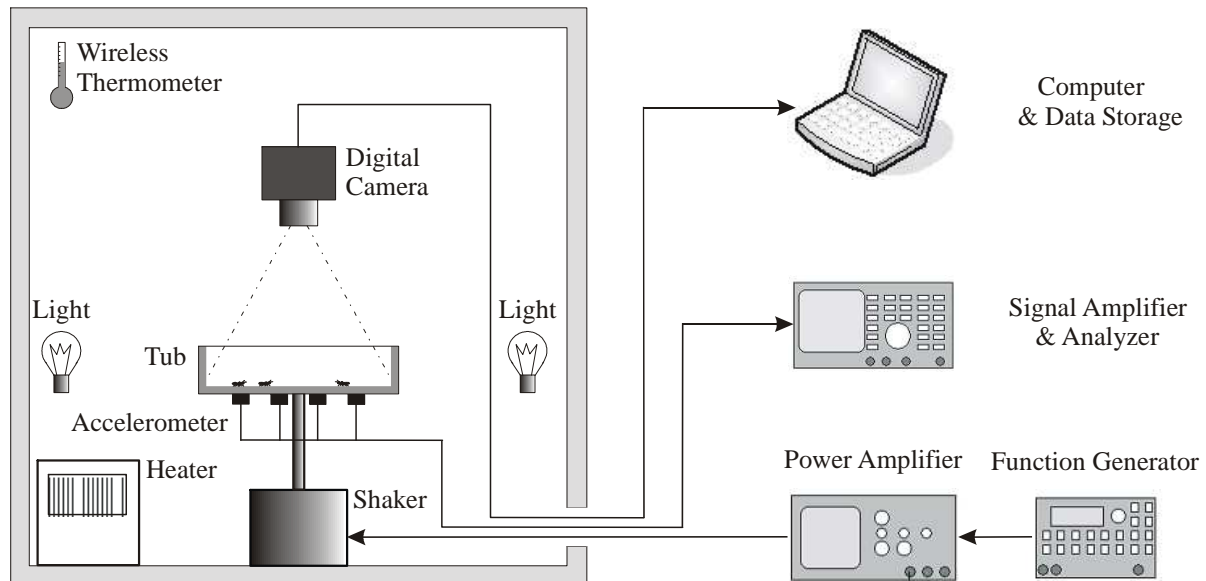
PIV is an optical measurement technique for fluid flows seeded with tiny tracer particles [3-7]. In a standard PIV system a laser light sheet is used to illuminate a plane in the measured flow field. Image pairs are usually taken with a digital camera to record displacements of tracer particles in the plane during a selected time interval. Many different algorithms can be used to determine the particle image displacements in a digitized PIV recording pair so that the velocities of the flow tracers can be calculated. The velocity of a tracer particle reflects the fluid flow velocity around the tracer particle. The PIV technique can be modified and applied to the insect motion measurement. To fit PIV to the ant tests, the following factors should be considered: (1) Since the ant motion can be limited in a planar surface, the laser light sheet can be omitted. However, the shadow of the ants on the surface should be avoided because the size of an ant is much larger than a tracer particle. (2) To capture moving objects in a natural illumination situation, the digital camera should have a high sensitivity to the light so that a short enough shutter time can be used. (3) Without a planar illumination, the noise in the background that includes reflection, shadow and unexpected objects is recorded together with the images of ants. Therefore, image-processing techniques are required to extract ant images from the disturbed raw recordings. (4) Because the distribution density of ant images is much lower than that of the particle images in usual PIV recordings, a particle image tracking (PTV) algorithm should be used to determine the ant image displacements, thus, suitable methods are required to identify and track individual ant images. In the present work the first two factors, i.e. (1) and (2), were taken into account at the hardware selection and system setup, whereas the last two factors, i.e. (3) and (4), were considered by developing appropriate image processing methods and evaluation algorithms.

Many different algorithms have already been developed to track particle images in LID PIV recordings, e.g. [8-11]. In most PTV algorithms, the centers of particle images are identified to determine the particle image displacements, and the particle images are paired according to their relative position to spatially or temporally neighbored particle images. Because the images of tracer particles are usually very small, very few PTV algorithms use the information of particle size, brightness and shape. The authors constructed an image tracking technique for fire ants based on the method and algorithm used to determine the velocity of the buoyant solid particle in a water tank, i.e. the images of solid particles in the water tank were identified with a recursive digital filter, and they were tracked between frames according to the size, brightness, shape of the particle image [12, 13]. Since the fire ants have a similar size and fixed shape, the orientation angle was added to the two-

frame tracking function to improve the reliability of the algorithm. The image of background disturbances was extracted with averaging a group of image frames and removed from the individual image frame [14].

In this paper we shall at first introduce some details of the experiment. Then, the image processing method and evaluation algorithms will be described. Finally, typical test results will be presented and discussed.

Figure 1. Schematic illustration of experiment setup for fire ant tracking.



2. Experiment setup

As shown in Fig.1, a small isolated room measuring about $2 \times 2 \times 2 \text{ m}^3$ was used as the experimental chamber. A small space heater was used to regulate the ambient temperature to $26\text{--}28 \text{ }^\circ\text{C}$, which was monitored by using a remote wireless thermometer from outside of the chamber. As a play stage for fire ants, a plastic tub measuring $350 \times 190 \times 120 \text{ mm}^3$ was placed in an aluminum support frame, confining the perimeter of the base of the tub but allowing for general deformation of the bottom surface of the tub. The 120-mm sides of the tub were coated with Fluon[®] AD1 to prevent the ants from escaping. The $350 \times 190 \text{ mm}^2$ inner bottom of the tub was painted with grid lines of distance of 31.75 mm ($1 \frac{1}{4}$ inches) for vibration mode analysis and image calibration. Since the vibratory sensory organs of fire ants appear to be most sensitive to the acceleration of the substrate vibration [15], 12 accelerometers were attached to the outer bottom surface of the tub to monitor the vibration. The tub support frame was connected to the center insert of a shaker by a steel rod. The shaker was placed on a vibration absorbent pad in order to minimize the effects of ambient seismic energy. Four small halogen lamps served as light sources for imaging purposes, and they were placed to prevent shadows. A 10-bit CMOS digital camera with $17\text{-}\mu\text{m}$ pixels was attached to a tripod and fixed to a working distance of 600-mm to capture images of the fire ants before and after excitation. The CMOS camera has a memory big enough to save more than 1,200 frames in each of 10 separate zones, so that image groups of multiple tests can be acquired without pausing for data downloading. The camera acquired image

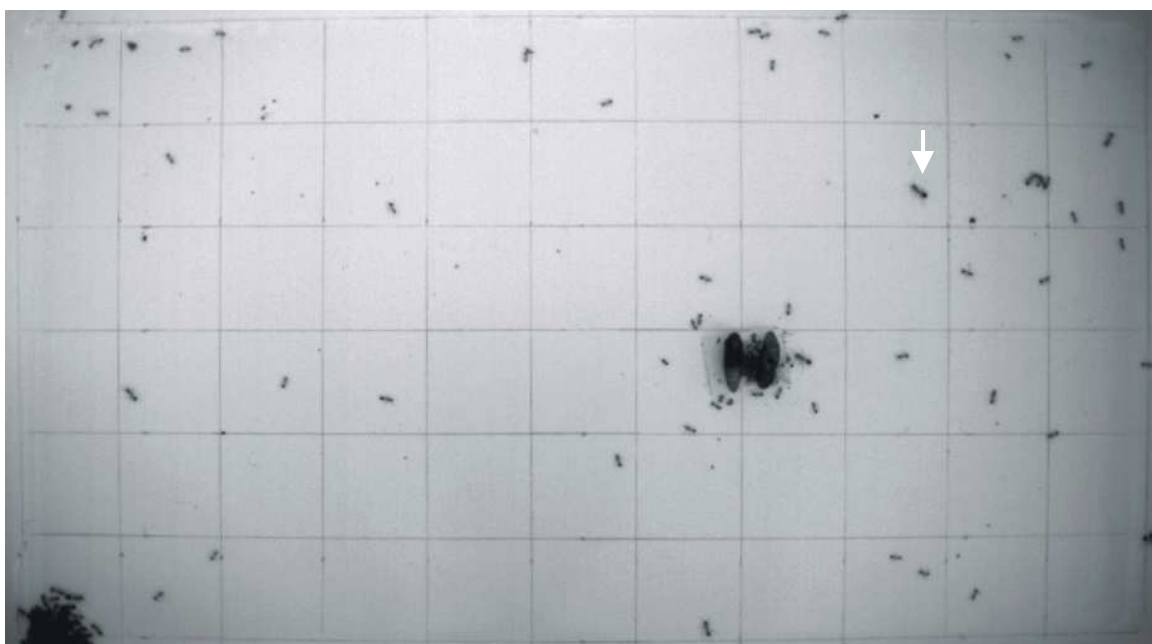
frames of 1024×512 pixels at a frame rate of 60 fps, which covered an area of 418×209 mm² in the objective plane with an imaging scale of 2.45 pixel/mm. The exposure time of 1/500 second allowed for sharp images of moving ants.

Other equipment components were placed outside of the room to minimize human interferences with fire ant behavior. The shaker was driven by the output of a power amplifier, and the vibration signals acquired at the tub bottom were amplified using low-noise amplifiers and processed using a dynamic signal analyzer. A computer was used to control the image acquisition and to download images after a test case was completed. Image processing and evaluation were completed offline.

200 workers of fire ants were collected and put into the tub for each test case. Acclimation to the new environment was allowed for 24 hours prior to commencement of experimentation, with drip irrigation providing a source of moisture. Lighting inside the chamber room was regulated by turning the lights on at ~ 8:00 AM every morning and then turning them off at ~ 5:00 PM to simulate the daylight cycle.

According to previous tests [16], the exciting frequency was selected to be 466 Hz to effectively stimulate the fire ants distributed on the tub bottom. Several groups of image frames were recorded for each test case: the first ant image recording group was taken one minute before the excitation as a reference. The second ant image recording group was acquired a few seconds after the ants were excited. The remaining 8 ant image recording groups were obtained at different time delays to observe the development of the ant motion within a one-hour period. Each image group has 1228 frames that were acquired at a rate of 60 fps in about 20 seconds. A sample image is shown in Fig.2. In this sample image, most of the ants cluster on the lower left corner of the image frame; some of the ants randomly distribute on the tub bottom; and a food source of two *Heliothis virescens* pupae is placed on the mid-high right.

Figure 2. Sample image taken at the bottom of the test tub: fire ants, food source, dusts, grid lines, and shadows are included.



3. Image processing and evaluation

3.1 Removing background disturbances

As shown in Fig. 2, the bottom of the tub is not uniformly illuminated, and the painted grid lines and unexpected objects like the food source, dust and dead ants are imaged together with the investigated active moving ants. The ant image recordings must be cleaned before being evaluated to ensure reliable and accurate results. The method described in [14] can be used to effectively extract the image of the constant background disturbances and to remove it from each ant image recording. Assume an ant image recording group has N frames, and the gray value distribution of each frame is represented as $G_k(x,y)$ ($k=1,2,3, \dots,N$). (x,y) is the position of each pixels in the image frame. The first step is to average all the frames to obtain an averaged gray value distribution as

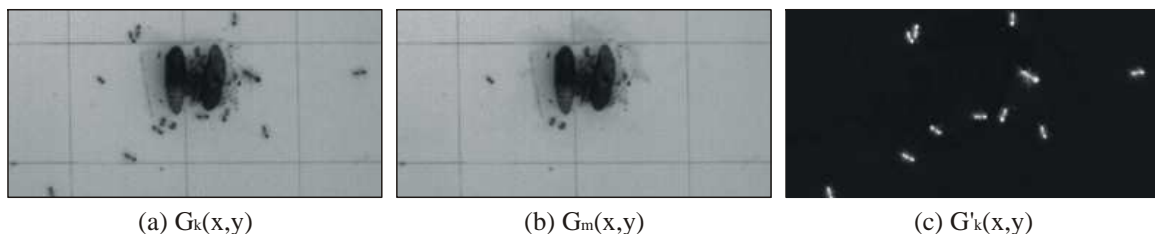
$$G_m(x,y) = \frac{1}{N} \sum_{k=1}^N G_k(x,y) \tag{1}$$

The second step is to subtract the averaged gray value distribution $G_m(x,y)$ from each image frame, i.e.

$$G'_k(x,y) = \begin{cases} G_m(x,y) - G_k(x,y) & \text{for } G_m(x,y) > G_k(x,y) \\ 0 & \text{for } G_m(x,y) \leq G_k(x,y) \end{cases} \tag{2}$$

Equation (2) is valid only when dark objects move in bright background, otherwise the images should be inverted. Fig.3 demonstrates the effect of the background removing determined by equation (1) and (2) for $N=1228$. Fig. 3a shows a part of a raw ant image recording of size of 256×128 pixels. In the raw image sample the grid lines, food resource, dead ants, and dust pieces are included. In the averaged image, i.e. Fig. 3b, some of the ant images disappear because they are images of active moving ants whose contribution to the averaged gray value is divided by 1228. When the background disturbances are removed by using equation (2), only images of active moving ants stay in the processed image frame, see Fig. 3c. Note that the ant images in Fig. 3c are inverted.

Figure 3. Sample images (256×128 pixels). (a) Raw image, (b) Averaged, (c) Cleaned.



3.2 Image identification

The tracking of individual ants between image frames is based on ant image identification, i.e. determination of the position and characters of each ant image. In order to complete image

identification, the processed digital image recording as shown in Fig. 3c is binarized according to a selected gray value threshold, so that the boundary of the ant image is fixed. The binary effect of the ant images is shown in Fig.4. In the presented case, the binarized ant images consist of teens to tens of square bright units (pixels of gray value 1) in the dark background (pixels of gray value 0). As schematically illuminated in Fig. 5, a multi-pass digital filtering is used to identify ant images. At first, as shown in the first picture from left, the bright units of the binary image are numbered one by one, whereas a great number (i.e. ∞) is given to pixels of the background. Thus, a two dimensional field of numbers $N(x,y)$ are obtained. Then, the number field is processed by using following recursive filter

$$N(x,y) = \min\{N(x+i,y+j); i = -1,0,1; j = -1,0,1\} \text{ for } N(x,y) \neq \infty \tag{3}$$

i.e. the number of each pixel in the field should be the minimum in the 3 by 3 neighborhood, except for those of pixels with number ∞ . To complete Equation (3), an iterated scanning of the number field is performed. The effect of the first scan of the above filtering is shown in Fig. 5 in the second picture from left. The 34 numbers in the first picture are reduced to 18 numbers in the second picture. The filtering with equation (3) is iterated until no changes can be made anymore in the number field. The final result is shown in Fig. 5 in the picture on the right, in which the pixels of each ant image have the same number that different from those of other ant images. The two ants in the 16×16-pixel image sample in Fig. 5 finally have number 1 and 9, respectively.

Figure 4. Sample image including 2 ants: (left) grayscale image, (right) binary image.

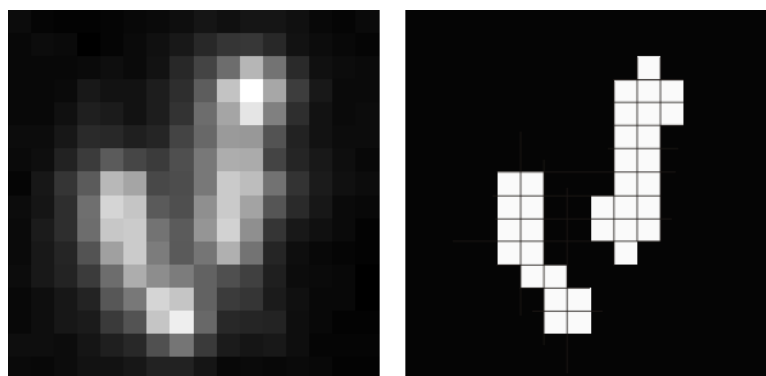
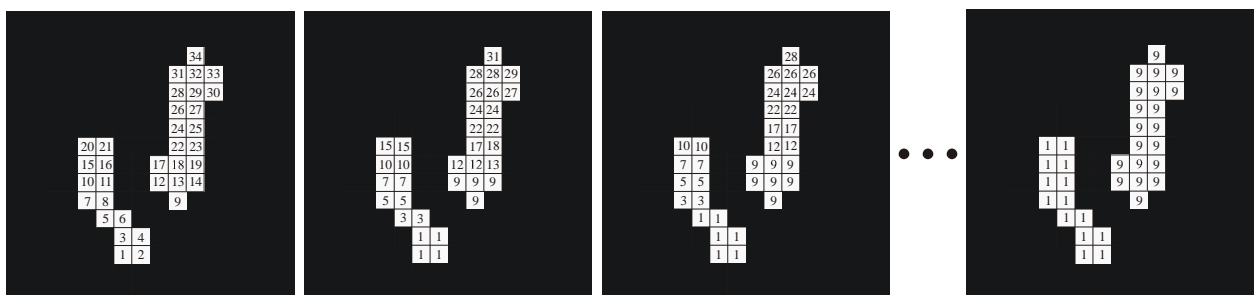


Figure 5. Schematic illumination of the image identification algorithm.



After the iterated filtering with equation (3), the total number of ant images (N_o), the number of pixels (i.e. size) of each ant image (S_n for $n=1,2,3, \dots, N_o$), and the position of each pixel for certain ant

image $((x_{n,i}, y_{n,i})$ for $i=1,2,3, \dots, S_n$) are determined, that directly enables a further determination of the position and brightness of the ant images as below.

Image center position:

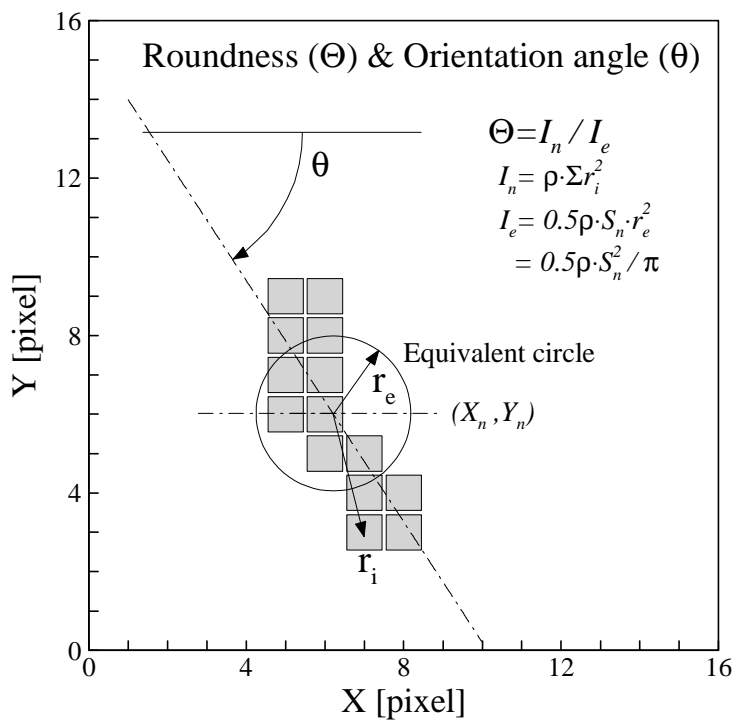
$$(X_n, Y_n) = \left(\frac{1}{S_n} \sum_{i=1}^{S_n} x_{n,i}, \frac{1}{S_n} \sum_{i=1}^{S_n} y_{n,i} \right) \tag{4}$$

Mean brightness:

$$B_n = \frac{1}{S_n} \sum_{i=1}^{S_n} G_k(x_{n,i}, y_{n,i}) \tag{5}$$

Wherein $G_k(x,y)$ is the gray value distribution of the original ant image recording as shown in Fig. 4a. The shape and orientation of the ant images can also be determined with the image identification results.

Figure 6. Roundness and orientation angle of ant image.



As shown in Fig. 6, the roundness (Θ) and orientation angle (θ) are used to represent the shape characters of an ant image. The main orientation of the ant image is determined by a least square linear fit of all the pixels of the ant image, and θ is the angle between the fitting line and the x-direction. The definition of the roundness is based on the definition of the moment of inertia for bodies with constant thickness in the axis direction and a uniform density distribution. Θ is the ratio of the moment of inertia between the ant image and the equivalent round body, i.e.

$$\Theta_n = \frac{I_n}{I_e} = \frac{\rho \sum_{i=1}^{S_n} r_i^2}{0.5\rho S_n^2 / \pi} = \frac{2\pi}{S_n^2} \sum_{i=1}^{S_n} [(x_i - X_n)^2 + (y_i - Y_n)^2], \tag{6}$$

wherein ρ is the mass of each pixel. Θ equals 1 for perfect round images, otherwise $\Theta > 1$. For square images the roundness Θ is about 1.05. There is no dominate orientation direction for round and square images, but the orientation angle θ become an important character when $\Theta > 1.05$.

3.3. Image tracking algorithm

Image tracking function:

Assume there are M_o and N_o numbers of ant images in the first and second frame of an ant image recording pair, and the image identification results for the two frames are represented as $\{X_{1,m}, Y_{1,m}, S_{1,m}, B_{1,m}, \Theta_{1,m}, \theta_{1,m} \text{ for } m=1,2,3\cdots,M_o\}$ and $\{X_{2,n}, Y_{2,n}, S_{2,n}, B_{2,n}, \Theta_{2,n}, \theta_{2,n} \text{ for } n=1,2,3\cdots,N_o\}$, respectively. A tracking function is defined as below to quantify the likeness of two ant images.

$$D(m,n) = c_s \left[\frac{S_{2,n} - S_{1,m}}{S_{1,m}} \right]^2 + c_B \left[\frac{B_{2,n} - B_{1,m}}{B_{1,m}} \right]^2 + c_\Theta \left[\frac{\Theta_{2,n} - \Theta_{1,m}}{\Theta_{1,m}} \right]^2 + c_\theta \left[\frac{\theta_{2,n} - \theta_{1,m}}{0.5\pi} \right]^2 \tag{7}$$

Wherein c_s, c_B, c_Θ and c_θ are weighting coefficients, which are determined according to experience in previous tests. Tracking function $D(m, n)$ describes a sum square difference of weighted variation rates of image size, brightness, shape, and orientation angle between image m in the first frame and image n in the second frame. The orientation angle θ may not be used in usual PIV for tracking spherical particles, e.g. [12], however, it may dominate the tracking because many ants have similar size and shape, and their images have the same brightness level.

Table 1. Example of ant image identification results.

<i>n</i>	<i>X</i>	<i>Y</i>	<i>S</i>	<i>B</i>	Θ	θ
1	30.33	4.33	15	170.1	1.86	-1.27
2	84.29	28.11	17	171.1	2.25	-0.37
3	176.43	45.68	16	166.7	2.39	-1.25
4	103.00	46.50	16	167.7	2.55	-0.62
5	149.56	56.81	16	172.9	2.95	1.23
6	133.53	55.66	15	163.9	2.60	0.05
7	167.62	83.31	39	169.4	2.69	-0.47
8	241.65	85.94	17	172.4	2.15	0.15
9	85.21	110.00	14	190.6	2.26	-1.20
10	89.50	114.00	20	176.4	2.00	1.41
11	155.50	122.25	16	171.5	2.63	1.55

Image tracking criteria:

The criteria to judge that image m' in the first frame and image n' in the second frame are images of the same ant is given as

$$D(m', n') = \min \left\{ \begin{array}{l} D(m', j) \text{ for } j=1,2,3 \dots, N_o \text{ and} \\ (X_{2,j} - X_{1,m'})^2 + (Y_{2,j} - Y_{1,m'})^2 \leq R_s^2 \end{array} \right\} \quad (8)$$

wherein search radius R_s is used to limit the search for the image partner n' in the neighbored area of the tracked image m' , so that some false tracking can be avoided and the computation time can be reduced.

Image tracking results:

The final results of the two-frame image tracking are position (X, Y) and displacement $(\Delta X, \Delta Y)$ of the tracked image pair, i.e.

$$\begin{cases} X(m', n') = (X_{2,n'} + X_{1,m'})/2 \\ Y(m', n') = (Y_{2,n'} + Y_{1,m'})/2 \\ \Delta X(m', n') = X_{2,n'} - X_{1,m'} \\ \Delta Y(m', n') = Y_{2,n'} - Y_{1,m'} \end{cases} \quad (9)$$

The speed of the ant is then determined by

$$\begin{cases} V_x(m', n') = \frac{\Delta X(m', n')}{\Delta t} \\ V_y(m', n') = \frac{\Delta Y(m', n')}{\Delta t} \end{cases}, \quad (10)$$

wherein Δt is the time interval between the two frames in the ant image recording pair.

Variation limits:

To validate an image tracking result, variation limits are set for all the tracking parameters, i.e.

$$\begin{aligned} \left| \frac{S_{2,n'} - S_{1,m'}}{S_{1,m'}} \right| \leq \phi_S, \quad \left| \frac{B_{2,n'} - B_{1,m'}}{B_{1,m'}} \right| \leq \phi_B, \\ \left| \frac{\Theta_{2,n'} - \Theta_{1,m'}}{\Theta_{1,m'}} \right| \leq \phi_\Theta, \quad \left| \frac{\theta_{2,n'} - \theta_{1,m'}}{0.5\pi} \right| \leq \phi_\theta. \end{aligned} \quad (11)$$

If ant image pair (m', n') does not fulfill the conditions described in equation (11), the tracking result is considered to be wrong. Limits ϕ_S , ϕ_B , ϕ_Θ and ϕ_θ are determined according to experience or an overall analysis of the digital ant image recordings.

Reversibility of image tracking:

Another way to validate an image tracking result is to conduct a reverse tracking. The reversed tracking function is defined as

$$D_r(m,n) = c_s \left[\frac{S_{1,m} - S_{2,n}}{S_{2,n}} \right]^2 + c_B \left[\frac{B_{1,m} - B_{2,n}}{B_{2,n}} \right]^2 + c_\Theta \left[\frac{\Theta_{1,m} - \Theta_{2,n}}{\Theta_{2,n}} \right]^2 + c_\theta \left[\frac{\theta_{1,m} - \theta_{2,n}}{0.5\pi} \right]^2 \tag{12}$$

If image pair (m',n') is determined with equations (8) but not fulfill condition

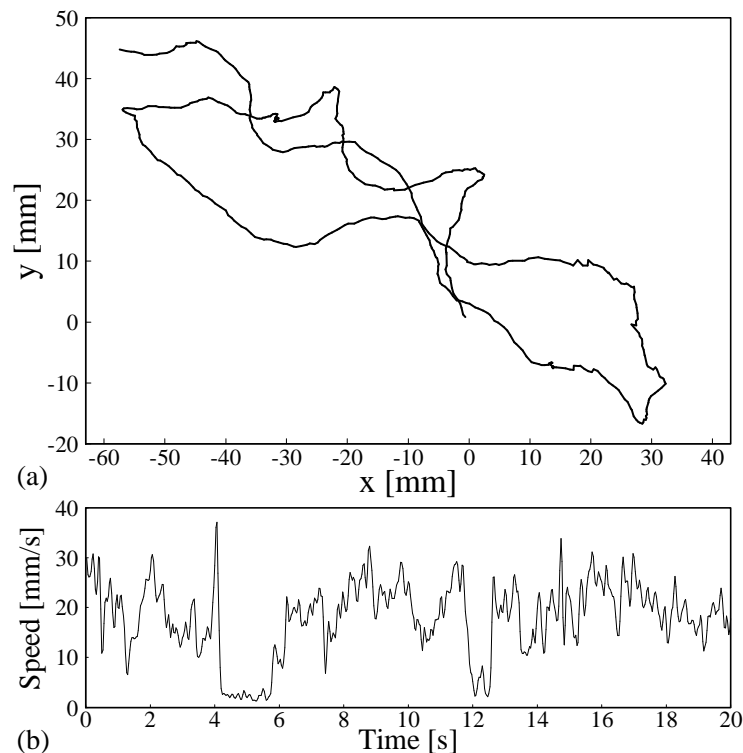
$$D_r(m',n') = \min \left\{ \begin{array}{l} D_r(i,n') \text{ for } i=1,2,3,\dots,M_o \text{ and} \\ (X_{1,i} - X_{2,n'})^2 + (Y_{1,i} - Y_{2,n'})^2 \leq R_s^2 \end{array} \right\}, \tag{13}$$

the tracking is not reversible. A tracking result without reversibility may be considered as a failure.

4. Experiment results

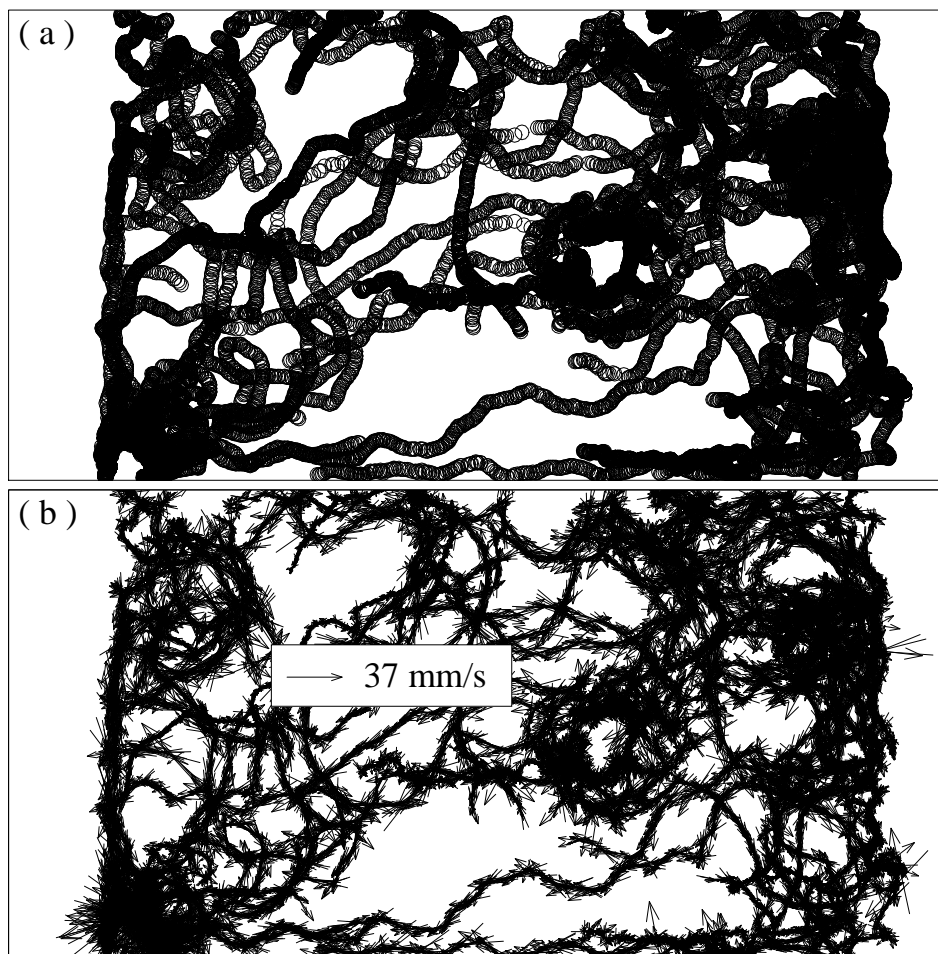
Two tests cases were conducted in two different days and the acquired data provides sufficient information for the test purpose. To effectively stimulate the fire ants distributed on the tub bottom, the exciting frequency was selected to be 466 Hz according to a previous investigation [16]. The excitation applied in the first case (case #1) resulted in the maximal acceleration amplitude of 0.72 m/s^2 near the tub center, whereas the exciting signal applied in second case (case #2) resulted in the maximal acceleration amplitude of 82.13 m/s^2 at the same position. Therefore, case #1 and case #2 were considered as a weak excitation and a strong excitation, respectively. Since the vibration of the tub bottom surface is perpendicular to the image plane and with limited amplitude, it does not have any obvious influence on the recording of fire ant motion.

Figure 7. Individual image tracking results: trail (a) and speed (b) of a selected ant in 20 seconds.



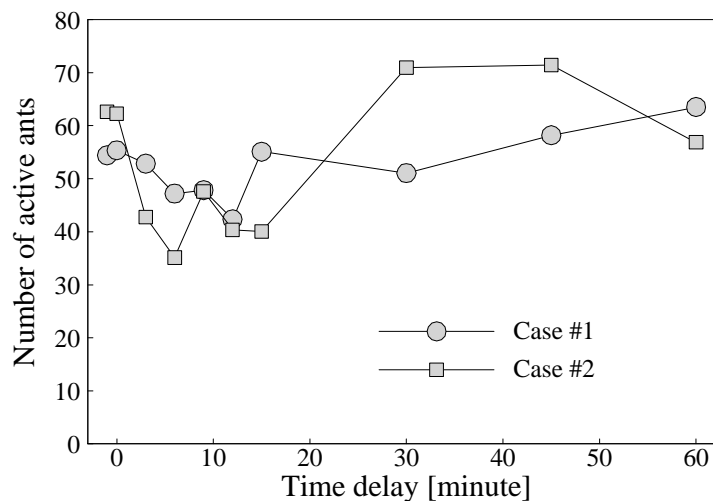
With the described image tracking technique the trail and speed of each active moving ant were determined in a 20-second data acquisition period. As an example, Fig. 7 shows the trail and speed time history of the ant indicated with a white arrow in Fig. 2, which belongs to the ant image recording group in case #2 for a few seconds after the excitation. Fig. 7a shows that the trail of the ant starts at position (0, 0), goes along a “∞” shape in a region of $90 \times 60 \text{ mm}^2$ in the 20-second period. In Fig. 7b the ant speed varies between 0 and 40 mm/s with a very complex distribution on time. The tracking results for a single ant enable study of the individual ant behavior. However, in the present work we concentrated on the overall behavior of the group of 200 ants. Fig. 8 displays the overlapped positions (8a) and speed vectors (8b) of identified 62 active moving ants in 1228 frames, which are evaluation results of the second ant image recording group for case #2. In Fig. 8a the trail of an individual ant can hardly be identified, however, the overlapped ant positions present a distribution of ant appearance probability in the observed area. Fig. 8b shows the corresponding ant moving speed vector at each ant position. Since so many vectors are overlapped, the speed of an individual ant cannot be seen clearly in the figure. In the current test case the constants in Eq. 7 were all set to 1, and those in Eq. 11 were all set to 2.

Figure 8. Ensemble image tracking results: overlapped ant positions (a) and speed vectors (b) in case #2, 2nd group (view area: $418 \times 209 \text{ mm}^2$).



The evaluation results are further processed, so that more useful information can be extracted from the available raw data. At first, the number of the active ants is investigated for the both cases at different delay time in the one-hour test period, and the results are given in Fig. 9. For each case the first symbol on the left represents the active ant number before excitation, and the second symbol, i.e. at “time delay”=0, represents data obtained a few seconds after the excitation. The followed eight symbols represent data obtained in the time period of restoration, i.e. 3, 6, 9, 12, 15, 30, 45 and 60 minutes after the excitation. As shown in Fig. 9, test results of both cases indicate that the number of active moving ants reduces after being excited by surface vibration of the tub, and it reaches to the minimum at around 10 minute of the time delay. After 30 minutes, the number of the active moving ants is back to normal, i.e. the number before excitation. After 40 minute the active ant number increases to a little higher than that of before excitation.

Figure 9. Number of active ants in two test cases during one-hour test period.



A probability density function (PDF) of ant moving speed is determined for each ant image recording group with about 36000 speed values as shown in Fig. 8b. The probability density functions (PDFs) of ant speeds determined before excitation, a few seconds after excitation, and 6 minutes after excitation are given in Fig. 10 and 11 for the two test cases, respectively. The PDFs of the two test cases are similar before the ants being excited, and only a little difference can be observed between 10 and 30 mm/s when they are plotted together. The undisturbed PDFs have a maximum near to 5 mm/s, and they reduce exponentially with increasing ant speed. It can be seen in Fig. 10 and 11 that the PDF of ant speed is obviously changed in a few seconds after the excitation, but it returns to the undisturbed distribution in about 6 minutes. The excitation of the tub surface vibration reduces the probability density of the low ant speed but increases that of the high ant speed. In order to clearly compare the changes of the PDFs between the two test cases, the PDFs of the undisturbed ant speed are subtracted from the PDFs of the ant speed determined a few seconds after excitation. The differences are shown in Fig. 12. The figure indicates that the excitation in case #1 increases the PDF of ant speed in the region of more than 10 mm/s, whereas the excitation in case #2 increases the PDF of ant speed for speed more than 20 mm/s. The increasing peak of the PDF is around 30 mm/s for both cases. As a direct consequence of the PDF increasing at the high speed end, the PDF decreases in the region of 0-9 mm/s

in case #1 and 0-20 mm/s in case #2. Obviously, the stronger excitation (i.e. in case #2) makes the moving ants a little more active, i.e. at a higher speed level.

Figure 10. Probability density functions of ant speed for Case #1 at three different test times.

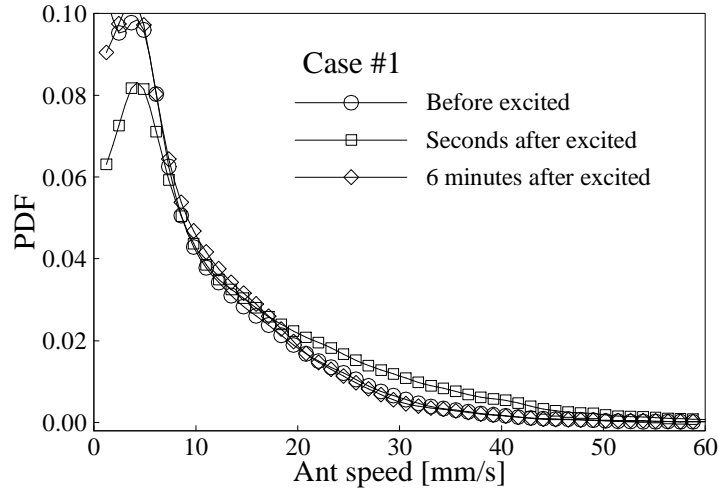


Figure 11. Probability density functions of ant speed for Case #2 at three different test times.

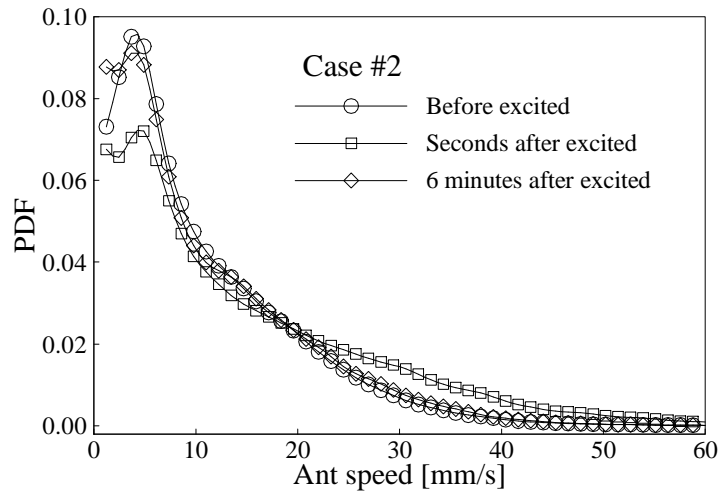
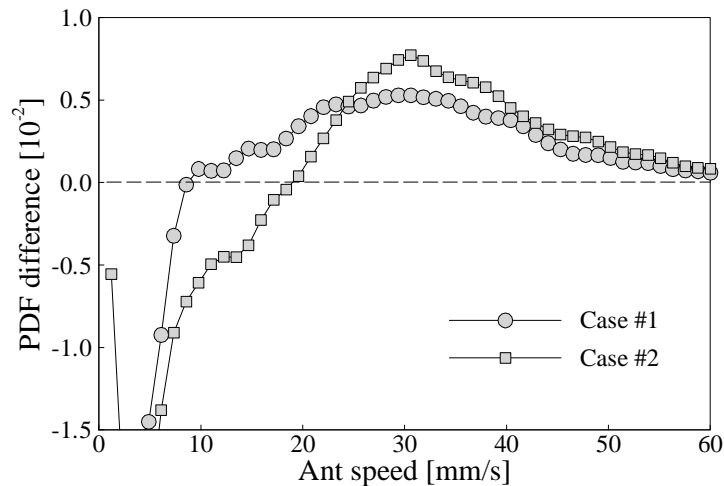


Figure 12. Probability density function differences in two cases.



5. Summary and conclusions

In this paper an image tracking algorithm is used to investigate moving fire ants on a planer surface. The digital images of fire ants are recorded with a high resolution video system, processed to remove the background disturbances, identified with a recursive digital filter, and tracked with their position, size, brightness, shape and orientation angles.

The fire ant image tracking is conducted in two ways, i.e. individual image tracking and ensemble image tracking. The individual image tracking is started with a selected fire ant at the first frame of a successively recorded image group. The selected fire ant image is tracked from frame to frame until it stops or goes out of the image frame. Since the individual fire ant image tracking may fail when two or more fire ants meet together, the tracked trail should be confirmed with a video playback. If the individual fire ant tracking is successfully completed, a position time history of the selected fire ant is determined and the speed variation can be investigated. The ensemble image tracking can be conducted with a minimum of two frames, and the speed values of a group of fire ants are determined for statistical analysis.

Tests were conducted with a group of 200 fire ant workers in a plastic tub. The test fire ants were excited with tub surface vibration of selected frequency and intensity. The experiment shows that, after acclimation to the environment for 24 hours, around three quarters of the ants keep calm in clusters, whereas about one quarter of the ants move actively. The speed of the active moving fire ants increases directly after the excitation, and return back to the normal level in about 6 minutes. The ant speed level is a little higher after a strong excitation than after a weak excitation. Experiment results indicate that the number of the active moving ants does not increase as expected after the excitation with substrate vibration, in the contrary, it decreases within 10 to 20 minutes after the excitation.

The application example demonstrates that the image tracking algorithm, which was originally described for tracking big buoyant particles in a water tank, can be effectively used to track images of moving fire ants on a planar surface with a necessary modification, i.e. including the orientation angle in the tracking function. The background image removing erases not only disturbances in the image background, but also images of fire ants that do not move, so that the active moving fire ants can be counted precisely. The used image identification method is effective but simple, so that it can easily be put into a computer program. The presented algorithm and method may be further improved with recent advancements in particle image velocimetry, e.g. [17-18], and used to track other insects moving on a planar surface.

References

1. Porter, S.D. Host Specificity and Risk Assessment of Releasing the Decapitating Fly (*Pseudacteon curvatus*) as a Classical Biocontrol Agent for Imported Fire Ants. *Biological Control* **2000**, *19*, 35-47.
2. Vogt, J.T. Light Intensity Affects Distribution of Attacking *Pseudacteon curvatus* (Diptera:Phoridae) in a Laboratory Rearing System. In *Proceedings of the 2002 Imported Fire Ant Conference*, Athens, Georgia, 2002; 16-20.
3. Merzkirch, W. Laser Speckle Velocimetry. In *Lasermethoden in der Strömungs-messtechnik*; Ruck, B., Ed.; AT-Fachverlag: Stuttgart, 1990; pp. 71-97.

4. Cenedese, A.; Paglialunga, A. Digital direct analysis of a multiexposed photograph in PIV. *Exp. Fluids* **1990**, *8*, 273-280.
5. Adrian, R.J. Particle-Imaging Techniques for Experimental Fluid Mechanics. *Annu. Rev. Fluid Mech.* **1991**, *23*, 261-304.
6. Willert, C.E.; Gharib, M. Digital Particle Image Velocimetry. *Exp. Fluids* **1991**, *10*, 181-193.
7. Grant, I. Particle image velocimetry: a review. *Proc Instn Mech Engrs.* **1997**, *211*, Part C, 55-76.
8. Chang, T.P.K.; Watson, A.T.; Tatterson, G.B. Image processing of tracer particle motions as applied to mixing and turbulent flow - I. The technique. *Chemical Engineering Science* **1985**, *40*(2), 269-275.
9. Okamoto, K.; Hassan, Y.A.; Schmidl, W.D. New tracking algorithm for particle image velocimetry. *Exp. Fluids* **1995**, *19*, 342-347.
10. Baek, S.J.; Lee, S.J. A new two-frame particle tracking algorithm using match probability. *Exp. Fluids* **1996**, *22*, 23-32.
11. Cowen, E.A.; Monismith, S.G. A hybrid digital particle tracking velocimetry technique. *Exp. Fluids* **1997**, *22*, 199-211.
12. Gui, L.; Hilgers, S.; Karthaus, A; Merzkirch, W. Ermittlung der Geschwindigkeits-verteilung von Feststoffpartikeln in einer Mehrphasenströmung mit Hilfe der Particle Image Velocimetry. In *5. Fachtagung von "Lasermethoden in der Strömungstechnik"*, Berlin, Sept. 11-13, 1996, 25.1-25.7.
13. Gui, L. Methodische Untersuchungen zur Auswertung von Aufnahmen der digitalen Particle Image Velocimetry. Dissertation, Universität Essen, 1998, Shaker Verlag: Aachen.
14. Gui, L.; Merzkirch, W.; Shu, J.Z. Evaluation of low image density PIV recordings with the MQD method and application to the flow in a liquid bridge. *Journal of Flow Visualization and Image Processing* **1997**, *4*(4), 333-343.
15. Mwangi, E.; Hasse, R.; Lago, P.; Buchholz, R. Vibrational sensitivity of tethered Black Imported Fire Ants (*Solenopsis richteri* Forel). In *International Conference on Acoustic Communication by Animals*, Maryland, July 27-30, 2003, 173-174.
16. Khoo, L.M.; Hasse, R.; Mantena, P.R. Structural dynamic analysis of phorid fly rearing tanks. In *ASME Region XI Technical Conference*, Miami, Florida, April 4-5, 2003, 1.1-1.8.
17. Raffel, M.; Willert, C.E.; Wereley, S.T.; Kompenhans, J. Particle Image Velocimetry - Practical Guide, 2nd Ed.; Springer-Verlag: Berlin, 2007.
18. Okamoto, K.; Nishio, S.; Saga, T.; Kobayashi, T. Standard images for particle-image velocimetry. *Meas. Sci. Technol.* **2000**, *11*, 685-691.